Methane – Natural Clay Interfacial Interactions as Revealed by High-Pressure Magic Angle Spinning (MAS) Nuclear Magnetic Resonance (NMR) Spectroscopy

Salim Ok *, David R. Cole, Julia M. Sheets, Susan A. Welch

Posted Date: 25 December 2024

doi: 10.20944/preprints202412.2193.v1

Keywords: Natural gas; shale gas; confinement; montmorillonite; kaolinite; methane; high-pressure NMR

 doi:10.20944/preprints202412.2193.v1

Article

Methane–Natural Clay Interfacial Interactions as Revealed by High-Pressure Magic Angle Spinning (MAS) Nuclear Magnetic Resonance (NMR) Spectroscopy

Salim Ok [1,2,*], Julia M. Sheets [1], Susan A. Welch [1] and David R. Cole [1,3]

[1] School of Earth Sciences, The Ohio State University, Columbus, Ohio 43210, USA
[2] Petroleum Research Center, Kuwait Institute for Scientific Research, P.O. Box 24885, Safat, 13109, Kuwait
[3] Department of Chemistry, The Ohio State University, Columbus, Ohio 43210, USA
* Correspondence: sok@uos.de

Abstract: The present study aims to provide fundamental, molecular- to microscopic-level descriptions of methane gas within natural source clay minerals. Texas montmorillonite (STx-1), Georgia kaolinite (KGa-2), and Ca^{2+} saturated Texas montmorillonite (Ca-STx-1, Ca-bentonite) were used as subsurface model systems for elucidating nano-confinement behaviors of ^{13}C labeled methane gas. High-pressure Magic Angle Spinning (MAS) Nuclear Magnetic Resonance (NMR) was utilized to characterize the interactions between methane and the clays by varying temperature and pressure. In the pure state, no significant thermal effect on the behavior of methane was observed. However, there was a perceptible change in the chemical shift position of confined methane in the mixtures with the clays up to 346 K. Conversely, the ^{13}C-NMR chemical shift of methane changed as a function of pressure in a pure state, and the mixtures with clays, attributed to the interaction of methane with the clay surfaces or the nanopore network of the clay-silica mixed phase. There was only one ^{13}C-NMR peak of methane in the mixture with either kaolinite (KGa-2) or Ca-bentonite with line-broadening compared to that of pure methane, but two peaks were observed in the mixture with STx-1, explained by the imbibition and mobility of methane in the pore network.

Keywords: natural gas; shale gas; confinement; montmorillonite; kaolinite; methane; high-pressure NMR

1. Introduction

There is a general agreement that the properties of bulk fluids are changed by solid substrates, confinement between two solid surfaces, or narrow pores due to the interplay of the intrinsic length scales of the fluid and the length scale due to confinement [1]. The behavior of fluids (i.e., gases and liquids) in confined geometries (pores, fractures) deviates from their bulk behavior in several ways [2,3]. Phase transitions (i.e., freezing and capillary condensation), sorption and wetting, and dynamical properties, including diffusion and relaxation, may be modified, with the most decisive changes observed for pores ranging in size from <2 nm to 50 nm—the micro- and mesoporous regimes [3]. Important factors affecting the structure and dynamics of the confined fluids include the average pore size and the pore size distribution, the degree of pore interconnection, and the strength of the fluid-substrate interaction. A quantitative understanding of the complex solid-fluid interactions under various thermodynamic conditions will influence the design of better substrates for technological applications (e.g., chromatography, fluid capture, storage and release, and heterogeneous catalysis) and gain insight into the essential energy-related environmental procedures (i.e., fluid and waste mitigation, carbon sequestration, gas shale recovery, etc.).

 doi:10.20944/preprints202412.2193.v1

Industry exploration and exploitation of shale gas (e.g., the Marcellus, Utica, and Barnett formations) have focused on understanding the fundamental behavior of volatile hydrocarbon—rock matrix interactions [4,5]. Hydrocarbon fluids, including methane (most abundant), ethane, and other longer chained alkanes, are stored in three forms: free gas in pores, free gas in natural fractures, and adsorbed on organic matter and silicate mineral surfaces [6]. The pores are typically submicron in size, cylindrical or slit-like shape, and commonly dominated by those as small as a few nm [7]. Understanding the molecular features of methane structure and dynamics in narrow silica-based pores might help quantify the molecular phenomena that occur during natural gas production following hydraulic fracturing. Several subsurface phenomena, including hydrocarbon migration, could be better understood and predicted once the adsorption and diffusion of hydrocarbons in narrow pores are clarified [8]. Gaining insight into methane behavior in narrow pores might have industrial applications, such as catalytic reactions. Moreover, revealing the characteristics of methane molecules in mixtures with natural clay might be useful in exploring "unconventional" shale gas reservoirs for large quantity production of natural gas [9].

1.1. Background and Objectives

In the recent contributions to understanding methane behavior under nanoconfinement relevant to subsurface energy systems, to overcome technical issues in mimicking the high-pressure conditions, the high-pressure magic angle spinning (MAS) nuclear magnetic resonance (NMR) method is employed in the current study [10,11]. High-pressure MAS NMR allows systematic investigation of methane dynamics in confined states at pressures such as 60 and 120 bar. In MAS, if the sample is spun at spinning frequencies in the range between 5 and 65 kHz [12], around an axis with an angle of 54.74° with respect to the static magnetic field, the anisotropy of nuclear interactions, exhibiting frequency dependence on the orientation according to a second order Legendre polynomial, is averaged out. Studying behaviors of gases by MAS NMR was rare [13] until the mid-2000s. In 2006, Deuchande et al. built a high-pressure insert made up of the polymer (poly ether ether ketone) (PEEK) [14]. Hoyt et al. [10] and Turcu et al. [11] improved the high-pressure MAS NMR technique by developing a unique gas loading chamber that permitted pressurization of the gas-tight rotors capable of hosting variable density gasses like methane and carbon dioxide (CO_2). Recently, the high-pressure MAS NMR technique has been utilized to investigate methane and/or CO_2 in mixtures with natural clays, including smectites [15,16], natural shale [17,18] and clay swelling in dry supercritical CO_2 [19].

In the current contribution, Texas montmorillonite from Gonzales County [20,21], was used as a subsurface model system for exploring the nano-confinement behavior of ^{13}C-labeled methane gas. Montmorillonite is a natural aluminosilicate having negatively charged layers balanced by cations [22]. The montmorillonite structure contains two tetrahedral sheets of silica and a central octahedral sheet. The sheets are connected by oxygen atoms shared by both sheets [23,24]. The unit layers are approximately 1-2 nm thick, and the clay minerals consist of micrometer-sized crystalline particles [25,26]. The clay mineral's layered structure has two surface types: edges and basal planes [27]. Due to surface activity and large surface area, clay minerals have been used in industrial catalysis, providing adsorption sites for gases such as methane [28,29].

Among different natural clays, Texas montmorillonite (STx-1) is known as dioctahedral, with low iron content [30]. Recently characterized STx-1 reportedly contains 73% smectite, ~25% silica (as cristobalite>tridymite>quartz) [31]. The study by Chipera and Bish [32] identified the silica as primarily opal-CT, a weakly ordered crystalline version of silica, plus 3% quartz + feldspar + kaolinite + talc(?) [32]. Referring to the literature, this mineral assemblage could be represented by an inter-grown pore network model [33]. According to this model, the pore network comprises pores and throats where the pores govern the storage of the confined fluid, while the throats direct the fluid flow during the production procedures. There could also be an irregular network of pores and pore throats [34]. Such network models motivate us to consider the silica could be intimately intergrown with the STx-1, resulting in a partially mixed ordered and disordered network system. In STx-1,

 doi:10.20944/preprints202412.2193.v1

quartz, silica, and carbonate minerals are considered contaminants. The octahedral sheet has a charge of -0.68 per formula unit, and the tetrahedral sheet has no permanent charge [35]. According to the report by Castellini et al. [31] STx-1 has a MgO concentration of 1.87 and CaO of 1.59 wt.%. Mg2+ is the main reason for the elevated permanent charge of STx-1 montmorillonite.35-36 According to the transmission electron microscopy (TEM) findings of Thao [36], the particle size of STx-1 could be categorized as follows: i) the bigger one with about 0.5 μm of thickness, moré, and curled edge particles, ii) the smaller one as thin, moré, and xenomorphic particles.

The other natural silicate of interest is kaolinite, which has a one-to-one aluminosilicate with two layers. The octahedrally coordinated aluminum layer is bridged to a tetrahedrally coordinated silicon sheet via oxygen atoms [27]. Kaolinite has no active layer, but OH groups are on the structure's surface [37]. The kaolinite sample from Warren County, Georgia (KGa-2) contains 96% kaolinite, 3% anatase, 1% crandallite, and mica and/or illite [32]. Kaolinite (KGa-2) has a zero tetrahedral charge and a positive octahedral charge of 0.16 e, probably from substituting Al3+ with Ti4+ in the octahedral sheet [35].

The present study aims to probe the fundamental, molecular- to microscopic-level behavior of the methane interaction with natural Earth minerals: montmorillonite, kaolinite, and purified Ca-bentonite, free of any natural metal carbonates **[38,39]**. Systematic high-pressure MAS NMR measurements have been conducted after carefully characterizing natural clay minerals to achieve this goal. Thus, we show how the behavior of methane changes in mixtures with high surface area clay minerals. In addition, how the available space in the clay mineral's interlayer structure might influence methane behavior is discussed based on experimental results. The controlled release experiment also reveals how methane mobility could be retarded by confinement within interlayers of montmorillonite.

2. Materials and Methods

2.1. Materials

Clay minerals were purchased from the Source Clays Repository, an entity of the Clay Minerals Society at Purdue University (West Lafayette, Indiana). Kaolinite sample was obtained from Warren County, Georgia, as high-defect kaolin (KGa-2), while montmorillonite was from Gonzales County, Texas (STx-1). The clay minerals' BET surface area values were measured with nitrogen adsorption and desorption at 77 K in liquid nitrogen with a Micromeritics ASAP 2020 surface area and porosity analyzer (Table 1). Before the adsorption-desorption measurements, kaolinite and montmorillonite were degassed at 423 K for 120 hours under a vacuum pressure of 10 μmHg.

Table 1. Surface areas of the clay minerals.

Sample Name	Specifications	Surface Area (m^2/g)
Texas Montmorillonite (STx-1)	Gonzales County, Texas, USA	75.0
Kaolinite (Georgia) (KGa-2)	Warren county, Georgia, USA	19.7

In addition, the Ca^{2+} saturated bentonite sample (Ca-STx-1) is purified from naturally occurring metal carbonate solids and has a < 2 μm fraction prepared by following the procedures in the literature [38,39]. Ca^{2+} saturation is also designed by suspending the clay in a 5M $CaCl_2$ solution for two weeks. The excess salt was removed by dialysis in deionized water. Furthermore, CO_2 intercalation into Ca-STx-1 was studied by in situ Attenuated total reflection Fourier Transform Infrared (ATR-FTIR) and in situ X-ray Diffraction (XRD) with anhydrous supercritical CO_2 [20]. The swelling property of Ca-STx-1 was also reported recently [21].

The morphology of the clays and silica (Figure 1(a–g)) was characterized by scanning electron microscopy using an FEI Quanta 250 Field Emission Gun scanning electron microscopy (SEM). SEM samples were prepared by depositing small quantities of the clay particles (without pre-treatment or

 doi:10.20944/preprints202412.2193.v1

grinding) on carbon tape mounted on aluminum stubs and then lightly coating with Au/Pd using a Denton Desk V sputter coater.

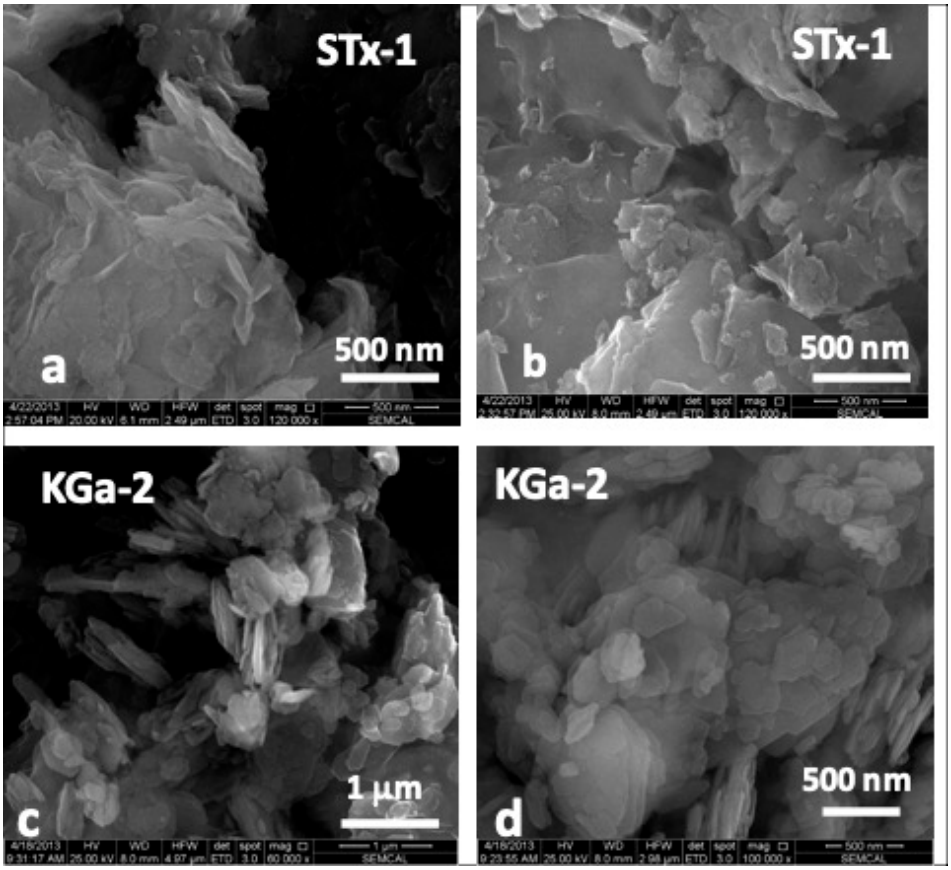

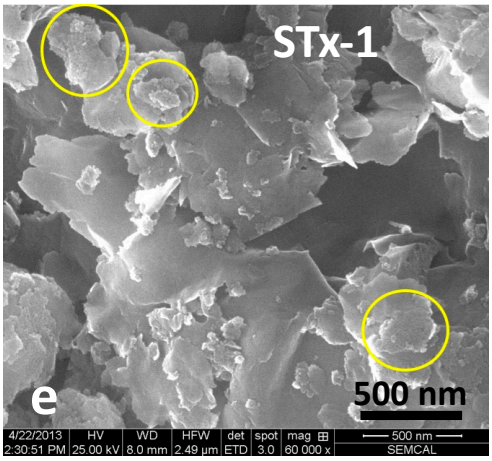

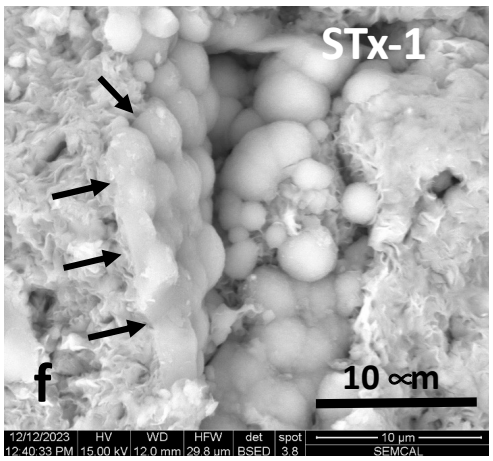

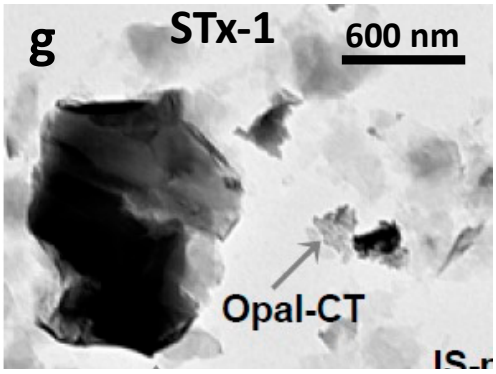

 doi:10.20944/preprints202412.2193.v1

Figure 1. Representative examples of Scanning (SEM) and Transmission Electron Microscopy (TEM) images: (a) & (b) SEM image of Texas montmorillonite (STx-1) and Georgia Kaolinite (KGa-2). (a) & (b) SEM images of STx-1 (Au/Pd coated on conductive carbon tape) depicting morphology of irregularly shaped variable size platy grains that occur individually or as clusters that can exhibit curling along the edges; (c) & (d) SEM images of KGa-2 (Au/Pd coated on conductive carbon tape) generally as clusters of plates and grains of diverse size revealing basal plane morphology; (e) varying size clusters of silica outlined in yellow circles dispersed among the STx-1; (f) more magnified view of the silica with "opal-like" spherical textural habit, in part, intimately connected with the montmorillonite (black arrows); and (g) Bright Field TEM image of STx-1 capturing one of the silica "opal-like" clusters revealing a mottled appearance (with permission of H-M Thao, 2006 Ph.D. dissertation [35].

2.2. Nuclear Magnetic Resonance: ^{13}C Direct Polarization (DP) and ^{1}H-^{13}C Cross Polarization (CP)

The high-pressure MAS experiments were performed on a Varian 300 MHz spectrometer operating at 75.4 MHz for the ^{13}C channel with 7.5 mm high-pressure specially designed rotors. Temperature calibration of the high-pressure probe was done by acquiring ^{207}Pb NMR spectra of lead nitrate as a function of temperature, as mentioned in the literature [40,41]. The details of the high-pressure chamber are explained elsewhere [10,11]. As explained previously [42], the samples for ^{13}C NMR spectra were loaded with pressures of approximately 30.0, 60.0, and 120.0 bar and at 323 K ± 1.0 K. Two temperatures were applied for studies at each pressure (307 and 346 K ± 1.0 K) for 13C NMR spectra resulting in internal sample pressures of 28.2, 56.4, 112.7, or 32.6 bar, 65.1 bar, 130.3 bar (±0.3 bar), respectively. Varying the pressure changed the density of methane and allowed the interrogation of the influence that phase change (gas to supercritical state) had on the fluid-silica interaction. The critical pressure (P_c) and critical temperature (T_c) of bulk methane are 45.992 bar and 190.564 K (−82.7 °C), respectively [43]. Thus, the temperature−pressure (density) regimes provided by the high-pressure MAS NMR method within the density regimes of shale gas systems are observed at the specified depths in the subsurface of the earth. The amount of methane used either in the pure state or in mixtures with the clays was determined by ultra-sensitive microbalance, taking the mass values before and after methane loading into the NMR rotors. The proton decoupled ^{13}C NMR spectra were acquired at 28.2 bar at 307 K, 32.6 bar at 346 K, 56.4 bar at 307 K, 65.1 bar at 346 K, 112.7 bar at 307 K, and 130.3 bar at 346 K. Varying the pressure produced a change in the ratio of the clay to methane gas. Moreover, to mimic a natural environment, the clay minerals (excluding Ca-STx-1 free from natural metal carbonates) were not exposed to further purification before the NMR measurements.

Further, switching the pressure from 28.2 to 56.4 bar or even to 112.7 bar allows changing the state from gas to supercritical state. The spinning frequency was 3 kHz. Proton-decoupled ^{13}C NMR spectra were acquired with 120 repetitions. Thus, the temperature-pressure (density) capabilities of the recently established high-pressure MAS technique are consistent with those identified for shale gas systems encountered at depth in the subsurface.

3. Results and Discussion

3.1. Natural Clay Characterization

3.1.1. BET

Table 1 summarizes the results of the BET measurements. Texas montmorillonite (STx-1) has a larger surface area than Georgia Kaolinite (KGa-2). The surface area of both clays is slightly lower than the values mentioned in the literature [27].

 doi:10.20944/preprints202412.2193.v1

3.1.2. SEM Measurements

The natural clay SEM images (Figure 1a–d) show morphology as clusters composed of irregularly shaped flakes often curled along the edges for STx-1 (Figure 1a,b) and basal plane morphology for KGa-2 (Figure 1c,d). Silica occurs as distinct assemblies of spherical grains generally clustered together (Figure 1e) and in intimate contact with the clay (Figure 1f). Our XRD characterization, coupled with the SEM images and associated Energy Dispersive X-ray (EDX) spectroscopy, would suggest this silica is more opal-like than cristobalite or tridymite, so for the purposes of this study, we will simply refer to it as "silica." Figure 1g comes from the work of Thao who used TEM to characterize a number of clays including STx-1, revealing a mottled appearance reflecting the spherical texture observed in the SEMs. In addition, detailed characterization of the reactive surface area of both clays has been done by solid-state NMR [27]. The details of the Ca-STx-1 properties can be found in the literature [20,21,38,39]. According to Leong et al. [35], STx-1 has a BET surface area of 83.8 m^2/g, while the BET surface area of KGa-2 is reported as 23.5 m^2/g. Widjaja and Inkiriwang also reported a BET surface area of 69.3 m^2/g for Ca-bentonite [44].

3.2. High-Pressure MAS NMR

Earlier NMR reports in the literature focused on the methane behavior at pressures below the P_c of methane [45–47]. The temperature and pressure ranges in our study are above methane's critical point values, allowing us to probe clay-supercritical methane interactions. The observations of the methane behavior in mixtures with clays demonstrate how the unique high-pressure MAS method helps follow the NMR shifts by temperature, pressure, composition, etc. The high-pressure MAS NMR46 gives maximal NMR sensitivity with low ^{1}H and ^{13}C background signals. MAS NMR also allows the collection of high-resolution spectra because the line-broadening arising from various internal and external nuclear interactions is averaged by the mechanical spinning of the samples **[10,11]**. In addition, anisotropic contributions to the ^{13}C-NMR spectrum of methane are also eliminated by MAS [45]. Thus, separate spectral components can be distinguished by rotating the sample at the magic angle and recording the proton-decoupled ^{13}C spectrum. In our previous high-pressure MAS-NMR study [42] of 4 nm nanoporous silica-methane interaction, we observed two distinct peaks, one like bulk methane and a second attributed to methane nanopore confinement. In the case of the silica-methane study, the bulk-like fluid could include the fluids between nanoporous particles and/or more free fluid in the centre of the 4 nm pores. It is hypothesized that methane confinement within a clay-silica pore network may exhibit a two-peak NMR spectrum. This outcome could potentially include variations in peak broadening and chemical shifts relative to adamantane, as observed through high-pressure MAS NMR spectroscopy.

3.2.1. Methane Interaction with Kaolinite: Role of Surfaces

Kaolinite is a non-expandable clay and, as such, acts as a control sample due to the absence of an accessible interlayer [48]. Methane molecules can interact only with the external surfaces of kaolinite, dominated primarily by aluminum hydroxide gibbsite-like layers. The kaolinite-methane spectrum exhibits a single ^{13}C NMR peak in Figure 2(a) with two distinct changes compared to bulk methane. There is a noticeable isotropic ^{13}C chemical shift of the mixture compared to the bulk fluid, ranging from 0.15 to 0.28 ppm depending on the temperature-pressure condition (Table 2). Further, there is a definite line broadening in the kaolinite-methane peak relative to bulk methane. The lack of an accessible interlayer does not result in two peaks as hypothesized for methane behavior associated with nanoconfinement. The observations can also be explained by susceptibility effects, where the broadened line-shapes are a result of inhomogeneities in the sample.

 doi:10.20944/preprints202412.2193.v1

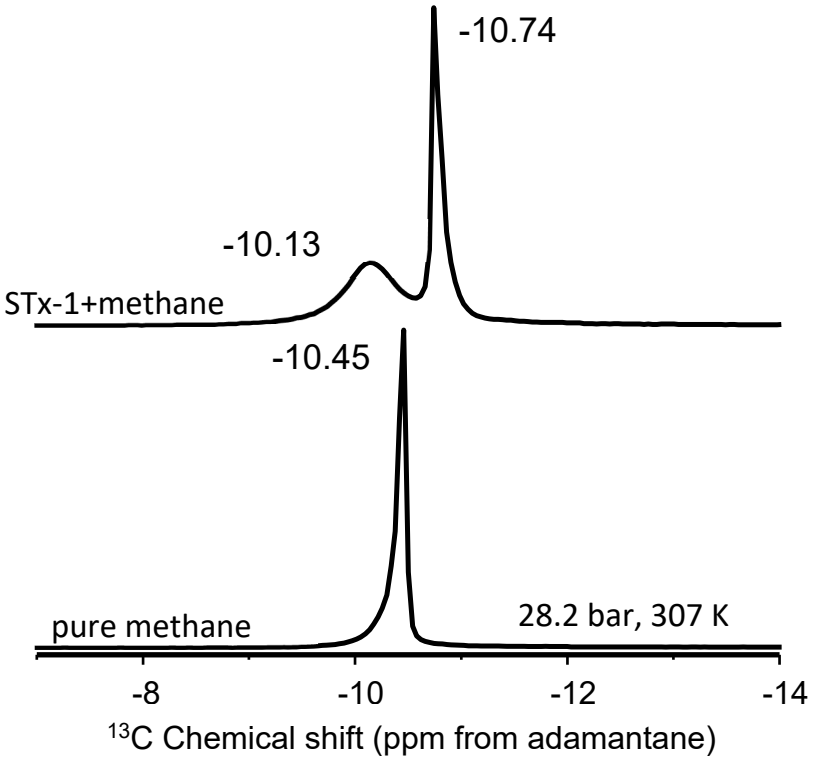

(a)

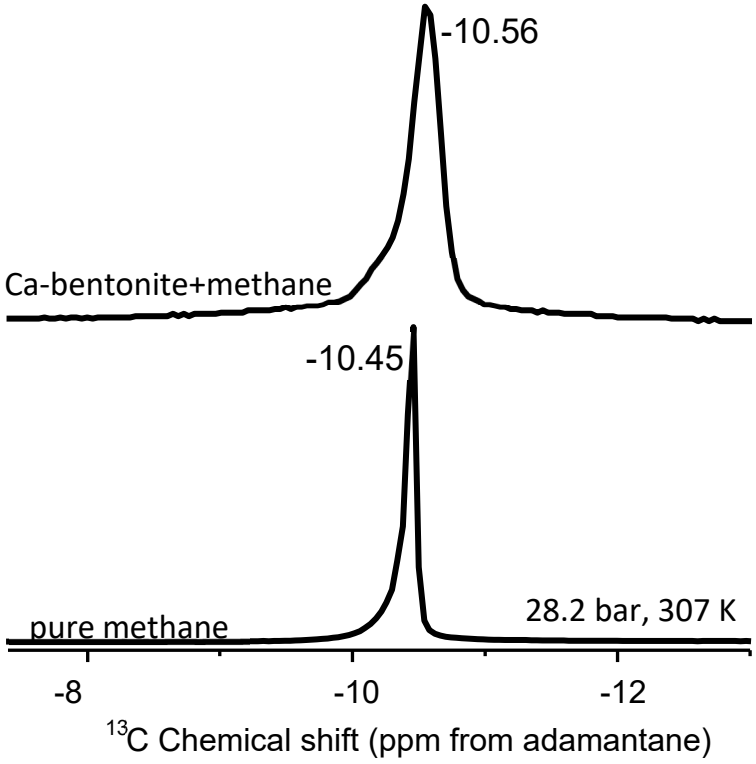

(b)

 doi:10.20944/preprints202412.2193.v1

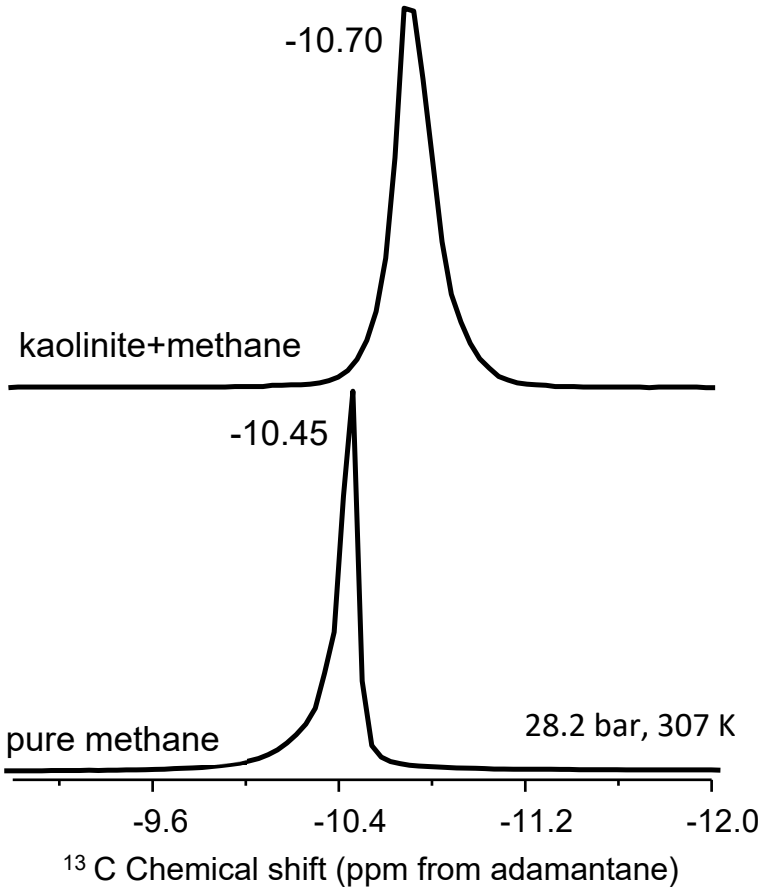

(c)

Figure 2. (a) Stack plot of proton decoupled ^{13}C NMR spectra of methane in the pure state and in mixture with montmorillonite (b) Stack plot of proton decoupled ^{13}C NMR spectra of methane in the pure state and in mixture with Ca-bentonite (c) Stack plot of proton decoupled ^{13}C NMR spectra of methane in the pure state and in mixture with kaolinite. The spectra were acquired at 28.2 bar and 307 K.

Table 2. Sample conditions, compositions, and measured ^{13}C isotropic chemical shift values of methane in the pure state and mixtures with clay minerals.

Sample	P (bar)	Temp (K)	bulk (ppm)	Interfacial (ppm)	amount of clay (mg)	amount of CH_4 (mg)
methane+Tx_Montmorillonite (STx-1)	28.2	307	-10.74	-10.13	0.2016	0.0057
microparticles	32.6	346	-10.71	-10.25	0.2016	0.0057
1-2 nm interlayer	56.4	307	-10.42	-9.89	0.2045	0.0192
natural clay	65.1	346	-10.41	-10.02	0.2045	0.0192
alumina + silicate (2:1)	112.7	307	-9.77	-9.42	0.2045	0.0405
	130.3	346	-9.77	-9.45	0.2045	0.0405
methane+Ca-Bentonite (Ca-STx-1)	28.2	307	-10.56		0.2950	0.0071
dried overnight under vacuum	32.6	346	-10.56		0.2950	0.0071
natural clay	56.4	307	-10.27		0.2950	0.0147
alumina + silicate+ including Ca (2:1)	65.1	346	-10.26		0.2950	0.0147
	112.7	307	-9.75		0.2950	0.0331
	130.3	346	-9.76		0.2950	0.0331
methane+kaolinite (KGa-2)	28.2	307	-10.70		0.2569	0.0064
dried overnight under vacuum	32.6	346	-10.70		0.2569	0.0064
natural clay	56.4	307	-10.48		0.2569	0.0137
alumina + silicate (1:1)	65.1	346	-10.48		0.2569	0.0137
	112.7	307	-9.86		0.1593	0.0365
	130.3	346	-9.90		0.1593	0.0365
pure methane	28.2	307	-10.45			0.0115
^{13}C labeled	32.6	346	-10.45			0.0115

 doi:10.20944/preprints202412.2193.v1

	56.4	307	-10.20	0.0226
	65.1	346	-10.20	0.0226
	112.7	307	-9.71	0.0452
	130.3	346	-9.71	0.0452

The -OH groups on the surface of the kaolinite may induce "dynamic order" to a portion of the methane molecules at the surface. Due to an exchange between the utterly free methane portion and the fraction interacting with the kaolinite surface, and because the motion of the methane molecules is averaged out on the NMR time scale, methane molecules experience an average of ^{13}C shielding since the exchange is fast compared to the NMR time scale; a lifetime average of shielding results in one signal in the spectrum [46].

3.2.2. Methane Interaction with Ca-Saturated Montmorillonite (Ca-bentonite)

Although the Ca-bentonite is an expandable clay at the nanoscale, its interaction with methane does not yield the two peak spectra as we hypothesized (Figure 2(b)). Rather, we observe a similar behavior as kaolinite wherein the single ^{13}C NMR peak exhibits line broadening compared to bulk methane, but where the half-width-at-half-maximum (HWHM) of the kaolinite peak is approximately 25% greater than the HWHM of Ca-bentonite. There is a much more subtle ^{13}C isotropic chemical shift than in kaolinite, ranging from 0.04 to 0.11 depending on the temperature and pressure (Table 2). For example, the delta value in the mixture with Ca-bentonite is only 0.05 ppm compared to bulk methane at the highest pressure of 130.3 bar at 346 K. Close inspection of the Ca-bentonite peak does reveal a subtle but perceptible shoulder on the less negative ^{13}C isotropic chemical shift side of the peak. The "subtle" shoulder be explained with a fraction of confined "methane", while the broadening of peaks in the absence of change of chemical shifts with respect to pure CH_4 could be attributed to the susceptibility of the clay.

3.2.3. Methane Interaction with Montmorillonite-Silica Assemblage

The interaction of methane and Texas montmorillonite (STx-1) yielded two distinct ^{13}C peaks (Figure 2c). The one more intense signal is derived from "bulk-like" fluid behavior, whereas the less intense peak is identified as "confined" methane **[42,49]** upon mixing methane with montmorillonite (Figure 2c). Unlike kaolinite and Ca-bentonite, there is no perceptible line broadening of the major peak. Previously, we observed two ^{13}C NMR signals in the mixtures of methane and 4 nm nanoporous engineered silica proxies, and a controlled release experiment also confirmed the "confined" methane resonance [42]. In the Koskela et al. [46] study of methane behavior in the gas state with mixtures of AlPO4-11, three ^{13}C-NMR methane signals were observed at temperatures above 250 K. The three components changed the NMR signal intensities dramatically with temperature. For instance, as the temperature increases, the signal from the adsorbed gas diminishes, while the signal from the free gas becomes more prominent [46].

Regarding the two peaks, it is essential to refer to Ok et al. [42] Figure 3 summarizes the study by Ok et al. [42], where methane was mixed with non-porous silica and ordered nanoporous silica with 200 nm average particle size and 4 nm pore diameter, respectively. There was only one ^{13}C NMR peak of methane observed when methane was mixed with non-porous silica. However, as methane was mixed with ordered nanoporous silica, there were two peaks of methane observed. The peak with higher intensity was assigned to confined methane in the nanopores of the silica with 4 nm pore diameter, while the other one with lower intensity was arising from "bulk-like" methane [42]. In the present study, we also observe two ^{13}C NMR peaks arising from methane, as methane was mixed with STx-1. Moreover, the peak explained by interfacial methane has lower intensity than that of the "bulk-like" methane. The difference in ^{13}C chemical shifts for methane confined in clay minerals versus ordered nanoporous silica can largely be attributed to the reference standard used in NMR spectroscopy (tetramethyl silane (TMS) vs. adamantane). TMS universally defines 0 ppm, while adamantane introduces a systematic offset due to its distinct chemical structure. Therefore, the use of adamantane can cause shifts to appear more negative as in the case of lower intensity peak in the

 doi:10.20944/preprints202412.2193.v1

present study. In Texas montmorillonite, the strong interactions between methane and reactive sites, such as hydroxyl groups, lead to greater deshielding and a more negative shift. The observed variations highlight the importance of reference selection in interpreting chemical shifts, consistent with findings in Ok et al. [42], where confinement effects were shown to influence NMR results significantly.

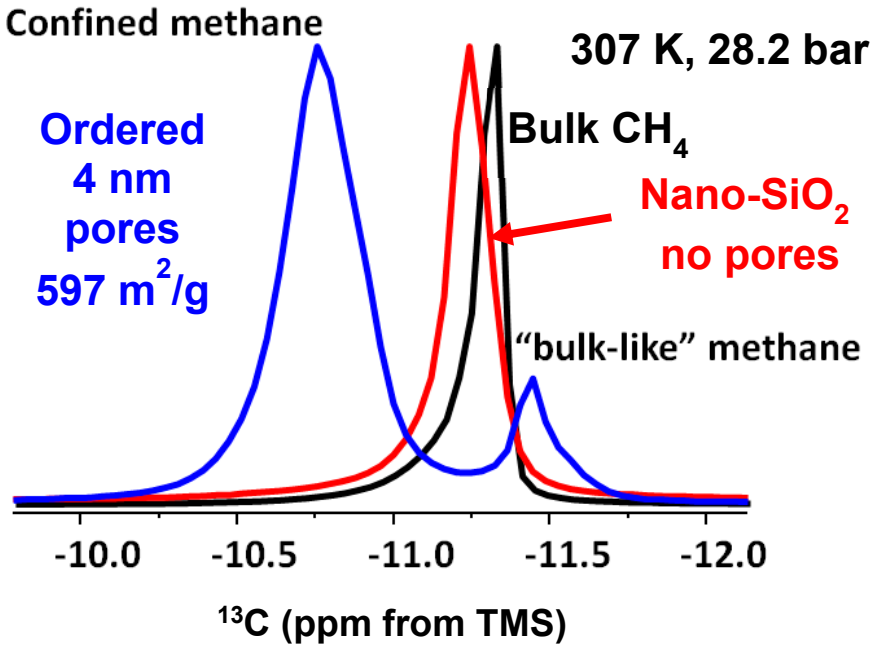

Figure 3. The stack plot of the ^{13}C NMR spectra of pure methane, methane in mixtures with non-porous silica, and in mixtures with ordered nanoporous silica with 4 nm pore diameter. The stack plot is prepared from Ok et al. [42], and the experimental details are given there. In the study by Ok et al. [42], tetramethyl silane (TMS) was used as reference. Copyright permission granted by American Chemical Society.

As described above, the STX-1 is a complex mixture of several phases dominated by montmorillonite and silica (opal-like in habit). The SEM images in Figure 1e,f show complex textural relationships between the clay and silica with an array of different types of nanoscale grain boundaries, including numerous pore throats and what appears to be intergrowth features. A non-trivial fraction of methane molecules could imbibe and move in this heterogeneous porous network. The nanoscale dimensionality of the network could confine methane molecules in a manner like how it was confined in 4 nm nanopores in the silica [42]. Further, we envision a smaller contribution to confinement from methane entering the clay interlayers and any pores in the silica. Opal and cristobalite are known to have complex microstructures that accommodate pores [50]. As a result, the nuclei of methane molecules have different shielding, which resulted in the two peaks detected by MAS NMR rather than a single peak that the limitations of static data acquisition would have produced [46].

3.2.4. Effect of Pressure and Temperature

Experiments varying pressure and/ or temperature were performed to better constrain the "bulk-like" and "confined" methane peak assignments by comparing the peak position and intensity. The full data set is given in Table 2. Figure 4a depicts the change in the ^{13}C chemical shift positions as a function of pressure from 28.2 to 112.7 bar at 307 K. Conversely, Figure 4b provides an example of the effect of temperature (307 versus 345 K) at approximately the same pressure (112.7 versus 130.3 bar).

Preprints.org (www.preprints.org) | NOT PEER-REVIEWED | Posted: 25 December 2024 doi:10.20944/preprints202412.2193.v1

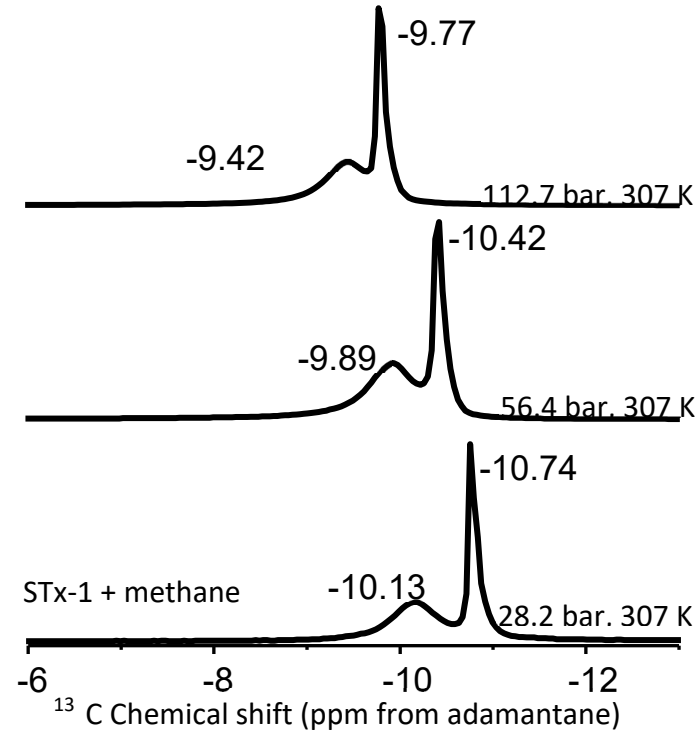

(a)

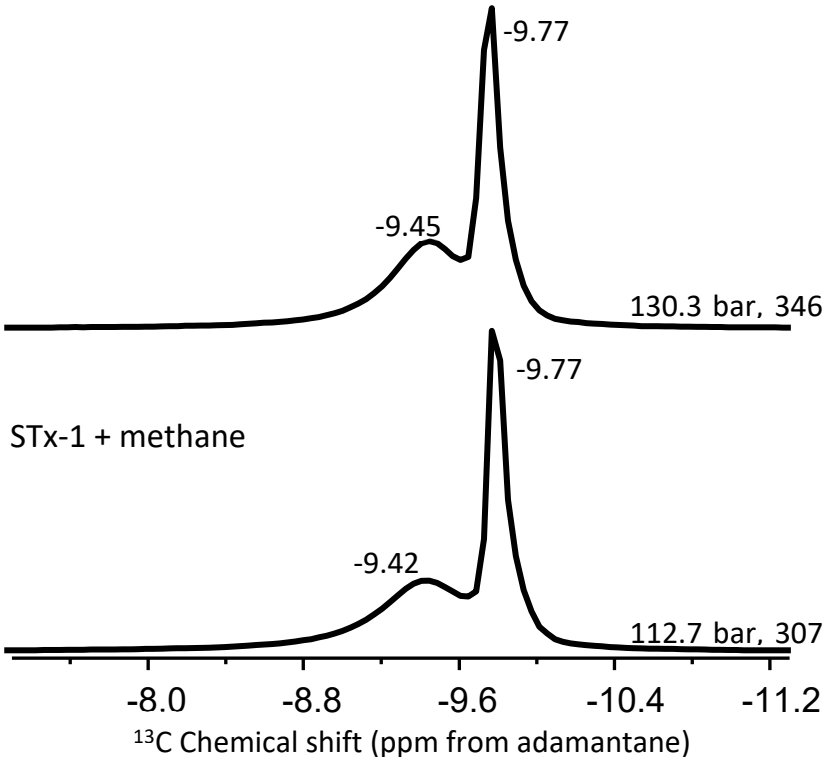

(b)

Figure 4. (a) Stack plot of proton decoupled ^{13}C NMR spectra of methane in mixture with montmorillonite acquired at a constant temperature of 307 K and pressures of 28.2 bar, 56.4 bar, and 112.7 bar (b) Stack plot of proton decoupled ^{13}C NMR spectra of methane in mixture with montmorillonite acquired at a constant pressure of 28.2 bar and temperatures of 307 K and 346 K.

 doi:10.20944/preprints202412.2193.v1

Pressure induces shifts in the pure methane peak position: 0.25 ppm going from 28.2 to 56.4 bar at 307 K, and 0.47 ppm shift from 56.4 to 112.3 bar again at 307 K (Table 3). The change is around 0.32 ppm for "bulk-like" methane and 0.20 ppm for confined methane in a mixture with montmorillonite. However, when the pressure is increased to 130.3 from 65.1 bar at 346 K, the shift is greater than 0.50 ppm for methane peaks in the mixture with montmorillonite. For example, the bulk-like methane peak depicted a 0.64 ppm change in its position, while the confined methane had a 0.57 ppm shift. Such peak shift changes observed in the mixture of methane and montmorillonite exceed that of pure methane and are indicative of methane molecules interacting with reactive sites of the clay. The delta values summarized in Table 3 are in the same order as those observed in mesoporous silica systems [42].

Table 3. The change in ^{13}C isotropic chemical shift of methane as a function of pressure and temperature.

	delta (28.2 bar) @ 307 K	delta (32.5 bar) @ 346 K	delta (56.3 bar) @ 307 K	delta (65.2 bar) @ 346 K		
			delta (ppm)			
pure methane	0.25	0.25	0.51	0.49		
CH_4 + Texas montmorillonite (bulk-like)	0.32	0.30	0.65	0.64		
CH_4 + Texas montmorillonite (interfacial)	0.24	0.23	0.47	0.57		
	28.2 bar and 307 K	28.2 bar and 346 K	56.4 bar and 307 K	65.1 bar and 346 K	112.7 bar and 307K	130.3 bar and 346 K
			delta (ppm)			
D : (methane + Ca-Bentonite) - (pure methane)	0.11	0.11	0.07	0.06	0.04	0.05
D : (methane + Kaolinite) - (pure methane)	0.25	0.25	0.28	0.28	0.15	0.19

Delta (28.2 bar) is the increase in pressure from 28.2 bar to 56.4 bar at 307 K, while delta (32.5 bar) is the increase in pressure from 32.6 bar to 65.1 bar at 346 K.

Delta (56.3 bar) is the increase in pressure from 56.4 bar to 112.7 bar at 307 K, while delta (65.2 bar) is the increase in pressure from 65.1 bar to 130.3 bar at 346 K [41,42].

Data in Table 2 demonstrate the ^{13}C chemical shifts in baseline experiments with pure methane exhibit no apparent dependency in the temperature range studied between 307 K and 346 K for each of the three pressure groups – i.e., 28.2-32.6; 56.4-61.2; 112.7-130.3b. Both temperatures are well above the critical temperature of methane. Still, it undergoes a phase change from gas to supercritical at pressures above 45.992 b and an associated modest density decrease from 307 to 346 K.

Similarly, for the montmorillonite-methane mixtures, the "bulk-like" methane peak remains essentially unchanged as a function of temperature for a given pressure group. The less intense "confined" methane peaks exhibit a very slight temperature dependence for pressures at or below

 doi:10.20944/preprints202412.2193.v1

65.1 b, on the order of 0.12 -0.13 ppm. The confined peaks move up the field with increased temperature (Table 2). However, it is clear the magnitude of the change in the peak position of confined methane as a function of temperature is less than the effect of pressure on the chemical shift position. Our results are valid for the temperature range only up to 346 K.

The similarity in positions of the ^{13}C chemical shifts, intensities, and response to pressure and temperature change indicates that a higher intensity peak observed in the montmorillonite – methane system arises from "bulk-like" methane (Figure 4(b)), which is consistent with the literature [42,46,49]. Although there is only one ^{13}C NMR peak of methane observed upon mixing with Ca-bentonite and kaolinite, that single peak also yielded the same response as a function of pressure and temperature as in pure methane (see Table 2). The results are valid for those cases where methane occurs as a gas or supercritical fluid. Depending on the phase diagram of methane and the possible contribution of confinement into the interlayers of montmorillonite, the thermal effect may be more pronounced.

As noted in the literature, an equilibrium exchange between "bulk-like" and confined methane molecules is expected when introduced to mesoporous silica [42,46,49]. This equilibrium may result in a dynamic equilibrium between confined and "bulk-like" methane molecules, which can manifest when two distinct peaks are observed. Furthermore, increasing pressure may cause densification that alters the chemical shift positions. For example, the study by Wu et al. [51] on the wettability influence on the adsorption attitude of nanoconfined methane showed that the ratio of bulk methane to nanoconfined average density ranges from 0.55 to 0.71 by elevating pressure; adsorption peak density can increase up to 3 times by manipulating the solid-phase wettability effect, and the adsorption volume in organic-rich shale is 1.72 times than that in inorganic-rich shale. Due to the adsorption mechanism, the methane amount near the solid phase can reach 2−5 times that in its bulk state. We propose that similar densification might happen on the natural clay surface when methane is mixed with natural clays. This densification might be reflected as a change in the chemical shift position of methane in the ^{13}C NMR spectra.

3.2.5. Comparison with Other Systems

It is instructive to compare the ^{13}C chemical shift results from clay-methane interactions with others reported in the literature. The deviation of our data from the literature values is largely related to the differences in experimental conditions, such as higher pressures up to 130.3 bar applied in the present study. The reported value of the methane gas chemical shift is δ = -7.00 ppm [52]. In the CH_4/C_3H_8 gas mixture, the methane peak has a chemical change δ = -8.52 ppm [47]. The methane chemical shift value was recorded between 0.00 and 5.00 ppm in mixtures with either Al and Si-based molecular sieves, such as SAPO-11 or aluminophosphates (AlPO4-11) **[45,46]**. These molecular sieves have different arrangements of atoms and surface charges compared to the clays **[45,47,52]**. Further, the studies do not identify external or internal referencing **[45–47,52]**. In our contribution, the methane ^{13}C NMR signal is externally referenced to the adamantane ^{13}C NMR signal.

AlPO4-11 has no lattice charges or cations [45]. In SAPO-11 containing Al and Si, negative lattice changes are formed and compensated by cations distributed in the framework [10]. AlPO4-11 and SAPO-11 have the same framework structure of straight channels with elliptical cross sections and no interconnections. The current report has utilized expandable montmorillonite and nonexpendable kaolinite-type natural clays. Montmorillonite has an active surface area in the interlayers, while kaolinite has hydroxide groups on the external surfaces. Bentonite is also enriched with Ca^{2+} ions. These physical and chemical differences of subsurface natural clays used in the current study, in addition to external referencing to the adamantane signal, may contribute to the observed difference of chemical shift values of methane compared to the values reported in the literature.

Bowers et al. [19] studied methane behavior in mixtures with smectite (the natural San Bernardino hectorite) and revealed that the ^{13}C NMR peak of methane is around -10.4 ppm in bulk. Moreover, the methane resonance appears between -10.0 and -10.3 ppm at the site of external pores. Depending on the hectorite type, such as PbH, CaH, NaH, and CsH, the "interlayer" methane peak

 doi:10.20944/preprints202412.2193.v1

is observed around -6.0 ppm for PbH and CaH, and -8.2 and -7.8 ppm for NaH and CsH, respectively. In continuation of their efforts, Bowers et al. [16] observed three methane ^{13}C NMR peaks assigned to bulk, the ones in mesopores and the ones in nanopores. The bulk peak appears around -10.41 ppm, while the one arising from methane molecules in mesopores is seen around -10.34 ppm. Referring to these studies, we suggest that in the current study, the second ^{13}C NMR signal of methane in mixtures with STx-1 arises from the methane molecules inside interfacial space with mesopores [53] having different dimensions between 2 and 4 nm diameter [42]. The delta value between these two peaks is also consistent with our previous results, where the behavior of methane was studied in mixtures with nanoporous silica having a 4.0 nm pore diameter [42].

A critical consideration regarding nanoconfined geometry is the reduction in the symmetry of the ^{13}C labeled methane [45]. Natural clays have reactive sites [27]. The interactions of methane gas molecules with the charge-compensating protons of the reactive sites, such as –OH groups, are likely to contribute to the reduction of symmetry [45]. Methane adsorption on silica was studied by Fourier-Transform Infrared (FT-IR) by Wu et al [54] Adsorbed methane indicated three IR bands at 3008, 2904, and 1304 cm^{-1}. These bands were attributed to the V1 (2904 cm^{-1}), V3 (3008 cm^{-1}), and V4 (1304 cm^{-1}) modes of methane. The V1 band is forbidden from infrared vibration. The appearance of that band implies that the T_d symmetry of the methane molecule is distorted on the surface of silica. Further, the slight frequency shift (30 cm^{-1}) of OH stretching depicted a weak hydrogen-bonding interaction between hydroxyls and adsorbed methane [54]. Therefore, it is likely that the hydroxyl groups of natural clays reduce the symmetry of methane molecules, leading to line broadening and shifts in chemical shift. This change in chemical shift can be further understood in terms of the average electron density experienced by the ^{13}C nucleus. When the methane molecule interacts with the hydroxyl groups on the clay surface, the electron cloud distribution around the ^{13}C nucleus is altered due to the induced dipolar interactions and potential hydrogen bonding. These interactions reduce the electron density shielding the ^{13}C nucleus, leading to a shift in the observed resonance frequency. Such effects are a direct consequence of the altered local electronic environment caused by the adsorption of methane on reactive clay surfaces.

The other possible reason for observing the changes in chemical shift positions might be the inhomogeneous distribution of methane in the mixtures with natural clays and local magnetic susceptibility, as well as the magnitude of the response of NMR active nuclei to the applied magnetic field **[45,55,56]**. The interfacial interaction of methane within the silica matrix systems may also induce heterogeneity of the local magnetic susceptibility. Regions of different magnetic susceptibility [57] at the external surface of control kaolinite having -OH and methane may have local magnetic field strengths and Larmor frequencies, changing the position of the isotropic chemical shift of methane.

3.2.6. Rates of Methane Release

To better elucidate the nature of methane nanoconfinement in the montmorillonite/silica material, controlled pressure release experiments were conducted at the two temperatures, 307 and 346 K, and an initial pressure of 28.2 b (Figure 5a,b). The hypothesis is we should expect the “confined” methane to be released more slowly compared to the bulk methane and hence exhibit an observable difference in peak intensity versus time – i.e., with pressure decrease. Using peak heights from Figure 5a,b, estimates are made of the fractional change as a function of time for the four experimental scenarios – bulk and confined peaks at 307 and 346 K (Figure 6). The fractional change of peak height means how the volumes of confined versus bulk-like methane decrease as a function of time during the controlled release experiment.

 doi:10.20944/preprints202412.2193.v1

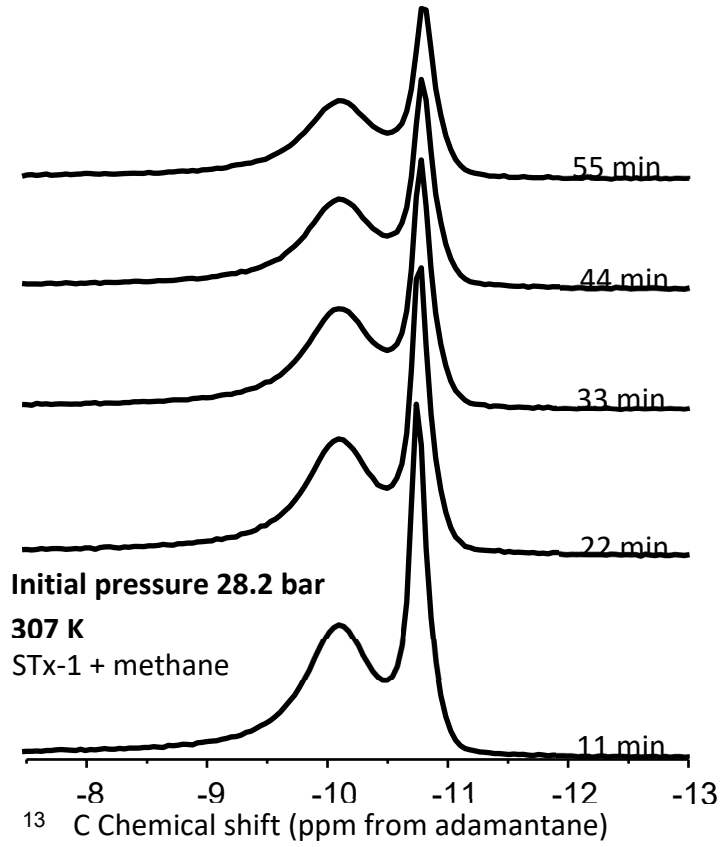

(a)

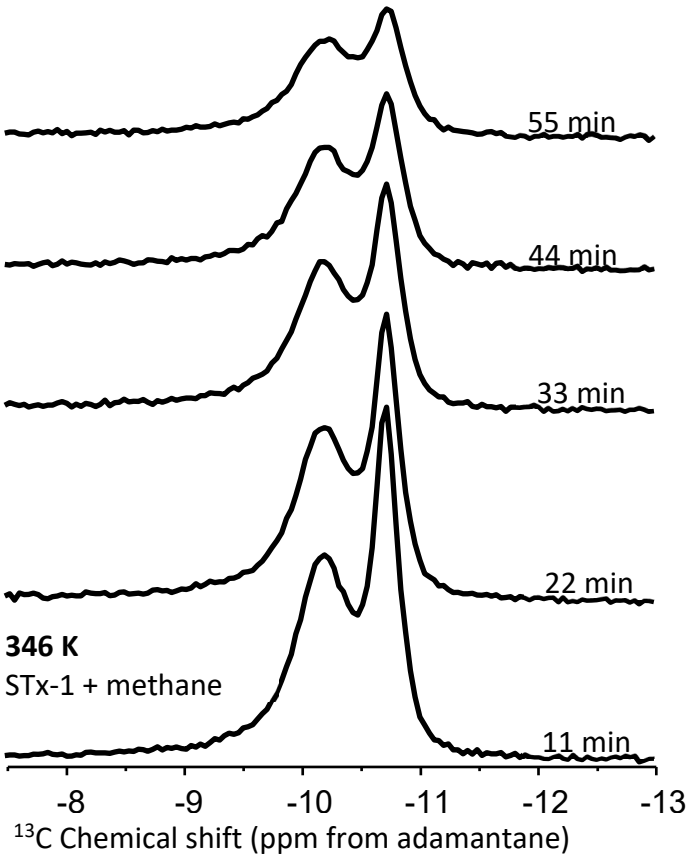

(b)

 doi:10.20944/preprints202412.2193.v1

Figure 5. Proton decoupled ^{13}C NMR spectra of methane in a mixture with montmorillonite acquired at 307 K (a) and (b) 346 K before and during the controlled release of methane as a function of time. The initial pressure was 28.2 bar.

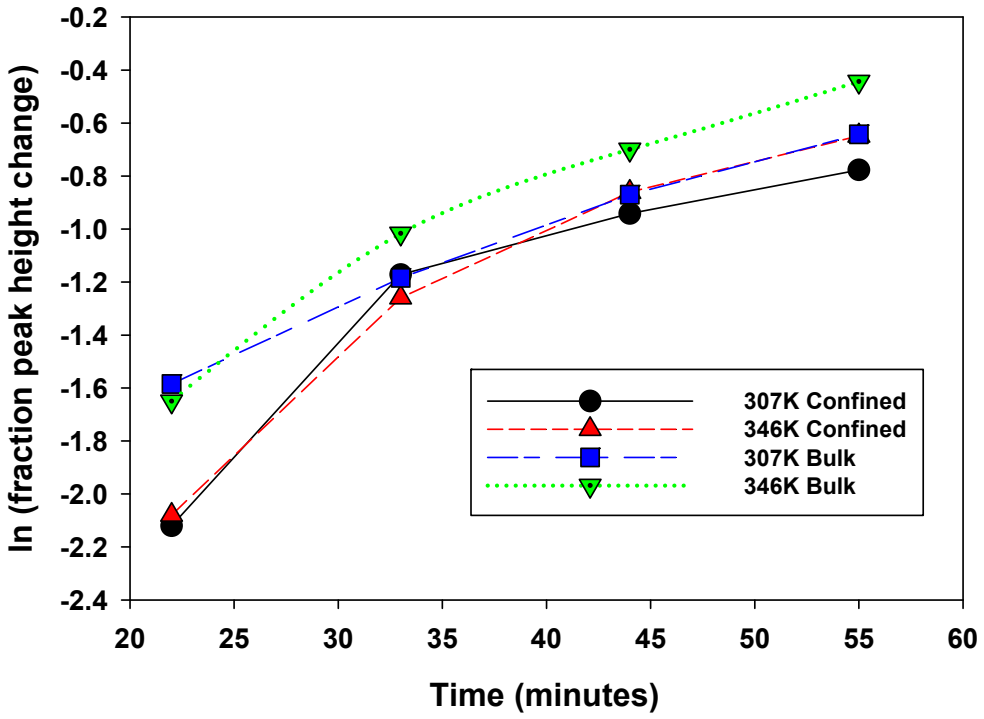

Figure 6. Change in peak height as a function of time during the controlled release experiment. Series 1: 307 K confined, Series 2: 346 confined, Series 3: 307K bulk, Series 4: 346K bulk.

Data in Figures 5 and 6 indicate the following trends:

(a) Peak intensities decrease for both types of peaks at both temperatures with increasing time as pressure is released (Figure 5(a,b)),

(b) At 22 minutes, there is a clear trend where the release rates of the bulk exceed those of the confined system- fractional change in peak heights of 0.2 versus 0.12, respectively,

(c) Overall, the fastest release rate is observed for the bulk fluid at 346 K.

(d) The slowest release rate is observed for confined peaks at 307 K.

(e) The difference between release rates for bulk 307 and confined at 346 is not easily distinguishable.

This data comparison indicates an observable difference in release rates between bulk and confined methane, as we have defined these. That said, this behavior is not unequivocal, as we do observe some overlap. This indicates that "confined" methane is released through the clay-silica pore network slower than "bulk-like" methane. Such a slower release rate of "confined" methane relative to "bulk-like" methane is consistent with the assignment of the two peaks. The confinement not only retards the release of the gas molecules, it also likely hinders the translational and rotational motion of any methane gas molecules imbibed in the interlayer space of montmorillonite. These results are roughly comparable to similar release experiments conducted using 4 nm nanoporous silica reported by Ok et al [42].

The other major issue in this controlled release experiment is how the confined fluid's density changes as time passes. Density plays a crucial role in several classical phase transitions. In the gas-liquid and liquid-solid transitions, density is the order parameter. In addition, when a fluid is confined, the phase behavior of the fluid is changed, and excluded-volume effects become apparent. For this reason, density fluctuations in confined geometry have been reported, for instance, for water

 doi:10.20944/preprints202412.2193.v1

[58,59] and cyclohexane [60]. Homogeneous density fluctuations of cyclohexane have been mentioned and attributed to thermal reasons [60]. However, in the present study, the controlled release experiment was performed isothermally, and the pressure was decreased as the methane molecules were released from the montmorillonite matrix. Hence, as time passes, the ratio of methane molecules per pore volume becomes smaller. This leads to a decrease in confined methane density. This change in the density of "confined methane" does not influence the chemical shift position of the "confined methane." Therefore, as listed in Table 4, the isotropic chemical shift of confined methane was not changed during the controlled released experiment.

4. Conclusions

Methane is an important component in natural gas [61], and combustion of methane has significance in energy production, practical applications, and for research purposes. Moreover, the recent increase in human population motivates researchers to find new energy resources [62]. In this regard, it is vital to research methane behavior at solid interfaces in confined state by mimicking natural environment. To fill that important gap of better understanding of methane behavior at solid interfaces in mixtures with natural clay minerals, the present study provides insight to the methane behavior in mixtures with clay minerals. In the pure state, no significant thermal effect was observed for the behavior of methane. A subtle change in the chemical shift position of confined methane in the mixtures with the clays up to 346 K was revealed by high-pressure ^{13}C-NMR. Interestingly, there was only one ^{13}C-NMR peak of methane in the mixture with either kaolinite (KGa-2) or Ca-bentonite with line-broadening compared to that of pure methane. Still, two peaks were observed in the mixture with montmorillonite (STx-1). Methane molecules can interact only with the external surfaces of kaolinite, with mainly aluminum hydroxide gibbsite-like layers. The interaction between methane molecules and the outer surfaces of kaolinite, with primarily aluminum hydroxide gibbsite-like layers, causes line broadening. This line broadening, compared to the isotropic shift position of pure methane in the 13C NMR spectrum, was accompanied by 0.15-0.28 ppm changes in the mixtures with kaolinite, but only 0.05 ppm change was observed in the mixtures with purified Ca-bentonite. There was a noticeable shoulder on the single peak for the Ca-saturated montmorillonite, suggesting the imbibition of a minor amount of methane in the interlayer.

The ^{13}C-NMR chemical shift of methane changed as a function of pressure. Moreover, two peaks are observed in the mixtures of methane with montmorillonite (STx-1). These two peaks are assigned as "bulk-like" and "confined." This is attributed to the densification of methane and the filling of the nanopore network present in the clay-silica mixture. The controlled pressure release experiments of methane interacting with Texas montmorillonite-silica STx-1 revealed a slower release rate of the confined methane, consistent with the sorption and densification in the complex nanopore network.

Author Contributions: Conceptualization, D.R.C. and S.O.; methodology, J.S., S.W., and S.O.; software, S.O., J.S., and S.W.; validation, D.R.C. and S.O.; formal analysis, D.R.C., S.O., J.S., and S.W.; investigation, D.R.C. and S.O.; resources, D.R.C.; data curation, D.R.C. and S.O.; writing—original draft preparation, D.R.C., S.O., J.S., and S.W.; writing—review and editing, D.R.C., S.O., J.S., and S.W.; visualization, D.R.C; supervision, D.R.C..; project administration, D.R.C. and S.O..; funding acquisition, D.R.C. All authors have read and agreed to the published version of the manuscript.

Funding: The A.P. Sloan Foundation provided support for S.O. sponsored Deep Carbon Observatory. D.R.C., J.S., and S.A.W. were supported by the Department of Energy, Basic Energy Sciences Geosciences Program under Grant DE-SC0006878.

Data Availability Statement: Not applicable.

Acknowledgments: The authors are grateful to David Hoyt from Pacific Northwest National Laboratory (PNNL) for the for the receipt of the Ca-montmorillonite sample as well as his help with the high-pressure MAS NMR measurements.

 doi:10.20944/preprints202412.2193.v1

Conflicts of Interest: The authors declare no conflicts of interest. The funders had no role in the design of the study; in the collection, analyses, or interpretation of data; in the writing of the manuscript; or in the decision to publish the results.

References

1. Gelb, L.D.; Gubbins, K.E.; Radhakrishnan, R.; Sliwinska-Bartkowiak, M. Phase Separation in Confined Systems. *Rep. Prog. Phys.* **1999**, *62*, 1573–1659.
2. Cole, D. R.; Striolo, A. The Influence of Nanoporosity on the Behavior of Carbon-bearing Fluids. In Deep Carbon: Past and Present; Cambridge University Press, 2019; pp 358–387.
3. Cole, D. R.; Ok, S.; Striolo, A.; Phan, A. Hydrocarbon Behavior at Nanoscale Interfaces. *Rev. Mineral. Geochem.* **2013**, *75*, 495–545.
4. Cole, D. R; Arthur, M. A. Unconventional Hydrocarbons. *Elements* **2014**, *10*, 257–296.
5. Striolo, A.; Cole, D. R. Understanding Shale Gas: Recent Progress and Remaining Challenges. *Energy & Fuels* **2017**, *31*, 10300−10310.
6. Ambrose, R.J.; Hartman, R.C.; Campos, M.D.; Akkutlu, I.Y.; Sondergeld, K. New Pore-scale Considerations for Shale Gas in Place Calculations. Soc. Petrol. Eng. 2010, 131772-MS, SPE Unconventional Gas Conference, Pittsburgh, PA, USA.
7. Ruhle, B.; Davies, M.; Lebold, T.; Brauchle, C.; Bein, T. Highly Oriented Mesoporous Silica Channels Synthesized in Microgrooves and Visualized with Single-molecule Diffusion. *ACS Nano* **2012**, *6*, 1948–1960.
8. Yethiraj, A.; A. Striolo, Fracking: What Can Physical Chemistry Offer? *J. Phys. Chem. Lett.* **2013**, *4*, 687–690.
9. Wang, H.-J.; Mutina, A.; Kausik, R. High-Field Nuclear Magnetic Resonance Observation of Gas Shale Fracturing by Methane Gas. *Energy & Fuels* **2014**, *28*, 3638−3644.
10. Hoyt, D.W.; Turcu, V.F.; Sears, J.A.; Rosso, K.M.; Burton, S.D.; Felmy, A.R., Hu, J.Z. High-pressure Magic Angle Spinning Nuclear Magnetic Resonance. *J. Magn. Reson.* **2011**, *212*, 378–385.
11. Turcu, R.V.F.; Hoyt, D.W.; Rosso, K.M.; Sears, J.A.; Loring, J.S.; Felmy, A.R.; Hu, J. Z. Rotor Design for High-Pressure Magic Angle Spinning Nuclear Magnetic Resonance. *J. Magn. Reson.* **2013**, *226*, 64–69.
12. Chen, P.-H.; Gao, C.; Price, L.E.; Urban, M.A.; Popp, T.M.O.; Barnes, A.B. Two Millimeter Diameter Spherical Rotors Spinning at 68 kHz for MAS NMR. *J. Magn. Res.* **2021**, *8–9*, 100015.
13. Miyoshi, T.; Takegoshi, K.; Terao, T. A Simple Method for ^{13}C CPMAS NMR Measurements under High Gas Pressures. *J. Magn. Reson.* **1997**, *125*, 383–384.
14. Deuchande, T.; Breton, O.; Haedelt, J.; Hughes, E. Design and Performance of a High Pressure Insert for Use in a Standard Magic Angle Spinning NMR Probe. *J. Magn. Reson.* **2006**, *183*, 178–182.
15. Bowers, G. M.; Schaef, H. T.; Loring, J. S.; Hoyt, D. W.; Burton, S. D.; Walter, E. D.; Kirkpatrick, R. J. Role of Cations in CO_2 Adsorption, Dynamics, and Hydration in Smectite Clays under In Situ Supercritical CO_2 Conditions. *J. Phys. Chem. C* **2017**, *121*, 577–592
16. Bowers, G. M.; Schaef, H. T.; Miller, Q. R. S.; Walter, E. D.; Burton, S. D.; Hoyt, D. W.; Horner, J. A.; Loring, J. S.; McGrail, B. P.; Kirkpatrick, R. J. ^{13}C Nuclear Magnetic Resonance Spectroscopy of Methane and Carbon Dioxide in a Natural Shale. *ACS Earth Space Chem.* **2019**, *3*, 324–328.
17. Bowers, G. M.; Loring, J. S.; Schaef, H. T.; Cunniff, S. S.; Walter, E. D.; Burton, S. D.; Larsen, R. K.; Miller, Q. R.; Bowden, M. E.; Ilton, E. S.; Kirkpatrick, R.J. Chemical Trapping of CO_2 by Clay Minerals at Reservoir Conditions: Two Mechanisms Observed by in Situ High-Pressure and -Temperature Experiments. *ACS Earth Space Chem.* **2019**, *3*, 1034–1046.
18. Loganathan, N.; Bowers, G. M.; Yazaydin, A. O.; Schaef, H. T.; Loring, J. S.; Kalinichev, A. G.; Kirkpatrick, R. J. Clay Swelling in Dry Supercritical Carbon Dioxide: Effects of Interlayer Cations on the Structure, Dynamics, and Energetics of CO2 Intercalation Probed by XRD, NMR, and GCMD Simulations. *J. Phys. Chem. C* **2018**, *122*, 4391–4402.
19. Bowers, G.M.; Loring, J.S.; Schaef, H.T.; Walter, E.D.; Burton, S.D.; Hoyt, D.W.; Cunnif, S.S.; Loganathan, N.; Kirkpatrick, R.J. Interaction of Hydrocarbons with Clays at Reservoir Conditions: in situ IR and NMR Spectroscopy and X-ray Diffraction for Expandable Clays with Variably Wet Supercritical Methane. *ACS Earth Space Chem.* **2018**, *2*, 640–652.
20. Loring, J.S.; Schaef, H.T.; Turcu, R.V.F.; Thompson, C.J.; Miller, Q.R.S.; Martin, P.F.; Hu, J.; Hoyt, D.W.; Qafoku, O.; Ilton, E.S.; Felmy, A.R.; Rosso, K.M. In Situ Molecular Spectroscopic Evidence for CO2 Intercalation into Montmorillonite in Supercritical Carbon Dioxide. *Langmuir* **2012**, *28*, 7125–7128.

21. Schaef, H.T.; Loring, J.S.; Glezakou, V.-A.; Miller, Q.R.S.; Chen, J.; Owen, A.T.; Lee, M.-S.; Ilton, E.S.; Felmy, A.R.; McGrail, B.P.; Thompson, C.J. Competetive Sorption of CO2 and H2O in 2:1 Layer Phyllosilicates. *Geochimica et Cosmochimica Acta* **2015**, *161*, 248–257.
22. Geist, M.F.; Boussois, K.; Smith, A.; Peyratout, C.S.; Kurth, D.G. Nanocomposites Derived from Montmorillonite and Metallosupramolecular Polyelectrolytes: Modular Compounds for Electrorheological Fluids. *Langmuir* **2013**, *29*, 1743–1747.
23. Zhu, R.; Chen, Q.; Liu, H.; Ge, F.; Zhu, L.; Zhu, J.; He, H. Montmorillonite as a Multifunctional Adsorbent can Simultaneously Remove Crystal Violet, Cetyltrimethylammonium, and 2-naphtol from Water. *Appl. Clay Sci.* **2014**, *88-89*, 33–38.
24. Bertuoli, P.T.; Piazza, D.; Scienza, L.C.; Zattera, A.J. Preparation and Characterization of Montmorillonite Modified with 3-aminopropylethoxysilane. *Appl. Clay Sci.* **2014**, *87*, 46–51.
25. Ji, L.; Zhang, T.; Milliken, K.L.; Qu, J.; Zhang, X. Experimental Investigation of Main Controls to Methane Adsorption in Clay-rich Rocks. *Appl. Geochem.* **2012**, *27*, 2533–2545.
26. Yeon, S.-H.; Seol, J.; Seo, Y.; Park, Y.; Koh, D.-Y.; Park, K.-P.; Huh, D.-G.; Lee, J.; Lee, H. Effect of Interlayer Ions on Methane Hydrate Formation in Clay Sediments. *JPCB Lett.* **2009**, *113*, 1245–1248.
27. Sanders, R.L.; Washton, N.M.; Mueller, K.T. Measurement of the Reactive Surface Area of Clay Minerals Using Solid-state NMR Studies of a Probe Molecule. *J. Phys. Chem. C* **2010**, *114*, 5491–5498.
28. Cheng, A.L.; Huang, W.-L. Selective Adsorption of Hydrocarbon Gases on Clays and Organic Matter. *Org. Geochem.* **2004**, *35*, 413–423.
29. Michalopoulos, P.; Aller, R.C. Rapid Clay Mineral Formation in Amazon Delta Sediments: Reverse Weathering and Oceanic Elemental Cycles. *Science* **1995**, *270*, 614–617.
30. Breen, C.; Moronta, A. Influence of Layer Charge on the Catalytic Activity of Mildly Acid-activated Tetramethylammonium-exchanged Bentonites. *J. Phys. Chem. B* **1999**, *103*, 5675–5680.
31. Castellini, E.; Malferrari, D.; Bernini, F.; Brigatti, M. F.; Castro, G. R.; Medici, L.; Mucci, A.; Borsari, M. Baseline Studies of the Clay Minerals Society Source Clay Montmorillonite STx-1b. *Clays Clay Miner.* **2017**, *65*, 220–233.
32. Chipera, S.J.; Bish, D.L. Baseline Studies of the Clay Minerals Society Source Clays: Powder X-Ray Diffraction Analyses. *Clays Clay Miner.* **2001**, *49*, 398–409.
33. Fatt, I. The Network Model of Porous Media. I, II & III, Petrol. Trans. Aime. 1956, 207, 144–177.
34. Kewen, W.; Ning, L. Numerical Simulation of Rock Pore-throat Structure Effects on NMR T2 Distribution. *Appl. Geophys.* **2008**, *5*, 86–91.
35. Leong, Y.-K.; Liu, P.; Au, P.-I.; Clode, P.; Liu, J. Microstructure and Time-dependent Behavior of STx-1b Calcium Montmorillonite Suspensions. *Clays Clay Miner.* **2021**, *69*, 787–796.
36. Thao, H.-M. Ph.D. Thesis. Characterization of Clays and Clay Minerals for Industrial Applications: Substitution non-Natural Additives by Clays in UV Protection. Greifswald, Germany, 2006.
37. Bhattacharyya, K.G.; SenGupta, S.; Sarma, G.K. Interactions of the Dye, Rhodamine B with Kaolinite and Montmorillonite in Water. *Appl. Clay Sci.* **2014**, *99*, 7–17.
38. Ilton, E.S.; Schaef, H.T.; Qafoku, O.; Rosso, K.M.; Felmy, A.R. In situ X-ray Diffraction Study of Na+ Saturated Montmorillonite Exposed to Variably Wet Supercritical CO_2. *Environ. Sci. Technol.* **2012**, *46*, 4241–4248.
39. Schaef, H.T.; Ilton, E.S.; Qafoku, O.; Martin, P.F.; Felmy, A.R.; Rosso, K.M. In situ XRD Study of Ca2+ Saturated Montmorillonite (STX-1) Exposed to Anhydrous and Wet Supercritical Carbon Dioxide. *Int. J. Greenhouse Gas Control* **2012**, *6*, 220–229.
40. Bielecki, A., Burum, D.P. Temperature Dependence of 207Pb MAS Spectra of Solid Lead Nitrate. An Accurate, Sensitive Thermometer for Variable-Temperature MAS. *J. Magn. Reson. Series A* **1995**, *116*, 215–220.
41. Langer, B.; Schnell, I.; Spiess, H.W.; Grimmer, A.-R. Temperature Calibration under Ultrafast MAS Conditions. *J. Magn. Reson.* **1999**, *138*, 182–186.
42. Ok, S.; Hoyt, D.W.; Andersen, A.; Sheets, J.; Welch, S.; Cole, D.R.; Mueller, K.; Washton, N.M. Surface Interactions and Confinement of Methane: A High Pressure Magic Angle Spinning NMR and Computational Chemistry Study. *Langmuir* **2017**, *33*, 1359–1367.
43. http://webbook.nist.gov/chemistry/fluid/
44. Widjaja, B.; Inkiriwang, C. B., Empirical Correlations among Liquid Limit, Clay Fraction, and Specific Surface Area for Kaolin and Calcium Bentonite Compounded Samples. Proc. of The Fifth Intl. Conf. On Advances in Civil and Structural Engineering - CSE 2016. pp. 42-44.

 doi:10.20944/preprints202412.2193.v1

45. Koskela, T.; Ylihautala, M.; Vaara, J.; Jokisaari, J. 13C NMR Spectroscopy of Methane Adsorbed in SAPO-11 Molecular Sieve. *Chem. Phys. Lett.* **1996**, *261*, 425–430.
46. Koskela, T.; Ylihautala, M.; Jokisaari, J.; Vaara, J. C-13 NMR of Methane in an AlPO4-11 Molecular Sieve: Exchange Effects and Shielding Anisotropy. *Phys. Rev. B* **1998**, *58*, 14833–14836.
47. Fleyfel, F.; Song, K.Y.; Kook, A.; Martin, R.; Kobayashi, R. Interpretation of C-13 NMR of Methane Propane Hydrates in the Metastable Nonequilibrium Region. *J. Phys. Chem.* **1993**, *97*, 6722–6725.
48. Loring, J.S.; Ilton, E.S.; Chen, J.; Thompson, C.J.; Martin, P.F.; Benezeth, P.; Rosso, K.M.; Felmy, A.R.; Schaef, H.T. In Situ Study of CO_2 and H_2O Partitioning between Na-Montmorillonite and Variably Wet Supercritical Carbon Dioxide. *Langmuir* **2014**, *30*, 6120–6128.
49. Ok, S.; Gautam, S.; Liu, K.-H.; Cole, D.R. Surface Interactions and Nanoconfinement of Methane and Methane plus CO_2 Revealed by High-Pressure Magic Angle Spinning NMR Spectroscopy and Molecular Dynamics. *Membranes* **2022**, *12*, 1273.
50. Bish, D. Personal communication.
51. Wu, S.; Luo, W.; Fang, S.; Sun, Z.; Yan, S.; Li, Y. Wettability Impact on Nanoconfined Methane Adsorption Behavior: A Simplified Local Density Investigation. *Energy & Fuels* **2022**, *36*, 14204−14219.
52. Jameson, A.K.; Jameson, C.J. Gas-Phase ^{13}C Chemical Shifts in the Zero-Pressure Limit: Refinements to the Absolute Shielding Scale for ^{13}C. *Chem. Phys. Lett.* **1987**, *134*, 461–466.
53. Ok, S. Low-field NMR Investigations on Dynamics of Crude Oil Confined into Nanoporous Silica Rods and White Powder. *Front. Chem.* **2023**, *11*, 1087474.
54. Wu, J.; Li, S.; Li, G.; Li, C.; Xin, Q. FT-IR Investigation of Methane Adsorption on Silica. *Appl. Surface Sci.* **1994**, *81*, 37–41.
55. Terenzi, C.; S.V. Dvinskikh, S.V.; Furo, I. Wood Microstructure Explored by Anisotropic H-1 NMR Line Broadening: Experiments and Numerical Simulations. *J. Phys. Chem. B* **2013**, *117*, 8620–8632.
56. Bonardet, J.L.; Fraissard, J.P. Method of Correcting Chemical Shifts of Adsorbate Molecules for Adsorbent Susceptibility. *J. Magn. Reson.* **1976**, *22*, 543–548.
57. Schurr, J.M. Phenomena Associated with Gel-Water Interfaces. Analyses and Alternatives to the Long-Range Ordered Water Hypothesis. *J. Phys. Chem. B* **2013**, *117*, 7653–7674.
58. Perret, E.; Nygard, K.; Satapathy, D.K.; Balmer, T.E.; Bunk, O.; Heuberger, M.; van der Veen, J.F. Molecular Liquid under Nanometre Confinement: Density Profiles Underlying Oscillatory Forces. *J. Phys.-Cond. Matt.* **2010**, *22*, 235102.
59. Zhang, Y.; Faraone, A.; Kamitakahara, W.A.; Liu, K.H.; Mour, C.Y.; Leao, J.B.; Chang, S.; Chen, S.H. Density Hysteresis of Heavy Water Confined in a Nanoporous Silica Matrix. *Proc. Natl. Acad. Sci. U.S.A* **2011**, *108*, 12206–12211.
60. Heuberger, M.; Zach, M.; Spencer, N.D. Density Fluctuations under Confinement: When is a Fluid not a Fluid? *Science* **2001**, *292*, 905–908.
61. Zettervall, N.; Fureby, C.; Nilsson, E. J. K. Evaluation of Chemical Kinetic Mechanisms for Methane Combustion: A Review from a CFD Perspective. *Fuels* **2021**, *2*, 210–240.
62. Lackner, M.; Fei, Q.; Guo, S.; Yang, N.; Guan, X.; Hu, P. Biomass Gasification as a Scalable, Green Route to Combined Heat and Power (CHP) and Synthesis Gas for Materials: A Review. *Fuels* **2024**, *5*, 625–649.